2D Tomographic Imaging of Active Sonar Echoes using a Non-Uniform FFT Technique.

Binh Nguyen (1), Hai-Tan Tran (2) and Shane Wood (1)

(1) Maritime Division, Defence Science and Technology Group, Third Ave - Edinburgh SA 5111, Australia
(2) Intelligence, Surveillance and Space Division, Defence Science and Technology Group, Third Ave - Edinburgh SA 5111, Australia

ABSTRACT

Two-dimensional (2D) sonar tomography is a technique used to obtain 2D images of underwater objects using a sequence of one-dimensional projections of the objects and a form of the so-called Back-Projection Algorithm (BPA). Two of the more popular approaches are the Polar-Coordinate BPA and the Rectangular-Coordinate BPA. In this paper we propose to use the 2D Non-Uniform Fast Fourier Transform (NUFFT) in a new form of the BPA to image underwater objects using sonar echoes. As usual for tomographic techniques, imaging performance is determined by the availability of sufficiently high-resolution projections and aspect coverage of the object. We demonstrate that the image inversion step based on the novel NUFFT can significantly improve imaging performance of sonar tomography in terms of image resolution, contrast and computational cost, in comparison to the two common approaches. The system requirements and data preparation are also discussed.

1 INTRODUCTION

For decades, sonar has been used for the detection, localization and classification of underwater objects. The effective use of active sonar requires the ability to distinguish between active sonar returns from underwater objects and clutter with acceptable levels of false alarms. One possible approach to address the challenge is to use 2D acoustic tomography.

2D tomography is generally a mathematical technique of reconstructing a 2D function from one-dimensional (1D) projections of the function at different aspect angles of the object of interest. It involves the Radon transform and image inversion algorithms in reconstructing the original function. In X-ray tomography, which is usually referred to as Computer Aided Tomography (CAT), the projections are density measurements based on material absorption. In radar tomography, which is based on reflective scattering phenomenology, the projections are range profiles, either in the down-range or cross-range directions. In sonar tomography, they can typically be limited to down-range projections. In the 2D reflection tomography method presented here, the object is effectively rotated while being ensonified by short sonar pulses (or pings). In radar tomography the bandwidth is relatively wide and subsequently a great deal of information can be captured in each projection and only a small coverage of aspect angle, typically less than 10°, is required to produce a useful image of an object. (Tran, Nguyen, at el, 2013). In contrast to this sonar signal bandwidth is often quite narrow resulting in relatively low target information content in sonar projections from each echo. Hence, a sufficiently large coverage of aspect angles in small steps is required to achieve a useful image of the target.

In 2D sonar tomography a very short sonar pulse is transmitted which is scattered off the target and recorded as a function of time delay, or propagation distance, at each aspect angle forming a projection. A collection of such projections from a wide enough range of aspect angles is input to an image inversion process to form an object image. One such an inversion process computes an inverse Fourier transform using polar-coordinates, which is also known as ‘filtered BPA’ or Polar-Coordinate BPA. Another method interpolates the scattering data into rectangular-coordinates, then performs a 2D inverse Fourier transform. Polar-Coordinate BPA is probably the simplest of the reconstruction methods conceptually and in terms of implementation while the Rectangular-Coordinate BPA may perform better than the Polar-Coordinate BPA but is sensitive to noise. Furthermore, aliasing of structures near the edges of the reconstruction region can occur due to polar-cartesian coordinate interpolation. (Monnig, Marshall, 1988).

The problem of irregularly spaced measurements is common in sonar operations. Irregular spaced measurements may be due to missing received signal caused by obstacles, noisy environments or faulty equipment. When receive data are non-uniform or unequally spaced in sampling, the classical FFT cannot be directly applied and alternative methods become necessary. Among these methods, the NUFFT is one of the most efficient motivating us to use it in the inversion step of the BPA.

In this paper a brief description of the three tomographic approaches namely, Polar-Coordinate BPA, Rectangular-Coordinate BPA and the NUFFT BPA is presented in Section 2. Section 3 describes an experimental demonstration and associated data pre-processing. Section 4 presents the experimental imaging results, while Section 5 discusses various issues of the proposed techniques and the experiment. Finally, some concluding remarks and future work are given in Section 6.

2 TOMOGRAPHIC IMAGE INVERSION TECHNIQUES

2.1 Polar-Coordinate BPA

The theory of BPA in polar-coordinates, also called 'filtered BPA', can be formulated as a general 2D Fourier analysis technique as follows. For a 2D real-valued function $q(x,y)$, as illustrated in Figure 1, the projection $p_\theta(r)$ along a line through the origin at angle θ, which is also called the Radon Transform, may be defined as

$$p_\theta(r) = \int_{-\infty}^{\infty}\int_{-\infty}^{\infty} q(x,y)\,\delta(x\cos\theta + y\,\sin\theta - r)dx\,dy, \tag{1}$$

where $\delta(x) = \begin{cases}+\infty & x = 0\\ 0 & x \neq 0\end{cases}$ is the Dirac delta function. It can be easily verified that the spatial Fourier transform $P_\theta(f_r)$ of $p_\theta(r)$, with spatial frequency in the *r*-dimension denoted as f_r, is a slice at angle θ, $Q_\theta(f_x,f_y)$, of the 2D Fourier transform of *q(x, y)*, i.e.,

$$\begin{aligned} P_\theta(f_r) &= \int_{r=-\infty}^{\infty} p_\theta(r)e^{-j2\pi f_r r}dr \\ &= Q_\theta(f_x,f_y), \end{aligned} \tag{2}$$

where, $f_x = f_r\cos\theta$, $f_y = f_r\sin\theta$, are the spatial frequency components in the *x* and *y*-dimensions along the slice at angle θ. This is the so-called Projection-Slice Theorem (Kak, Slaney, 2001). Once $Q_\theta(f_x,f_y)$ is constructed from many such slices over a sufficient range of aspect angles θ, $q(x,y)$ can be obtained from a 2D inverse transform; this is generally called the BPA.

$$\begin{aligned} q(x,y) &= \int_{-\infty}^{\infty}\int_{-\infty}^{\infty} Q_\theta(f_x,f_y)e^{j2\pi(xf_x+yf_y)}\,df_x\,df_y \\ &= \int_0^\pi \mathcal{F}^{-1}\{|f_r|\,P_\theta(f_r)\}_{(x\cos\theta+y\sin\theta)}d\theta. \end{aligned} \tag{3}$$

The subscript $(x\cos\theta + y\sin\theta)$ of the second line of equation (3) means the inverse Fourier transform, denoted by $\mathcal{F}^{-1}$, is calculated at $r = x\cos\theta + y\sin\theta$.

2.2 Rectangular-Coordinate BPA

In many sonar applications, measurements are naturally in polar-coordinates as the target changes aspect relatively to the sonar receiver. The Rectangular-Coordinate BPA is based on the use of a 2D Inverse FFT (2DIFFT) of the measurement samples in the frequency domain to obtain the target image, described in the first line of Equation (3). This requires an interpolation of the polar-format samples on to the rectangular grid samples as shown in Figure 2. This form of the BPA is sometimes called 'Convolution BPA'.

2.3 Non-Uniform FFT BPA

The NUFFT BPA technique is essentially the same as Rectangular-Coordinate BPA, except that the interpolation of samples to a rectangular grid is replaced by an efficient in-built interpolation scheme of the Non-Uniform FFT (NUFFT) (Greengard, Lee, 2004).

The NUFFT is an important and relatively recent algorithm. It is related to a discreet Fourier transform of an input signal of unequally sampled points which the normal FFT does not handle. The basis of the NUFFT algorithm is first to oversample the 2D FFT in both directions and then interpolate the Discrete Fourier Transform (DFT) coefficients onto the desired frequency locations as shown in Figure 3. The concept is similar to gridding for interpolation in frequency space. This algorithm is computed in O (N log N) operations rather than O (N^2) operations (Matej, Fessler, Kazantsev, 2003). There are several approaches in implementation of the NUFFT. In two dimensions, the algorithms of types 1 and 2 NUFFT are

$$F(k_1, k_2) = \frac{1}{N}\sum_{j=0}^{N-1} f_j e^{-i(k_1,k_2).x_j}, \tag{4}$$

$$f(x_j) = \sum_{k_1}\sum_{k_2} F(k_1, k_2) e^{i(k_1,k_2).x_j} \tag{5}$$

where $-\frac{M}{2} \leq k_1, k_2 < \frac{M}{2}$; M is number of samples, and $x_j \in [0, 2\pi] \times [0, 2\pi]$ (Greengard, Lee, 2004).

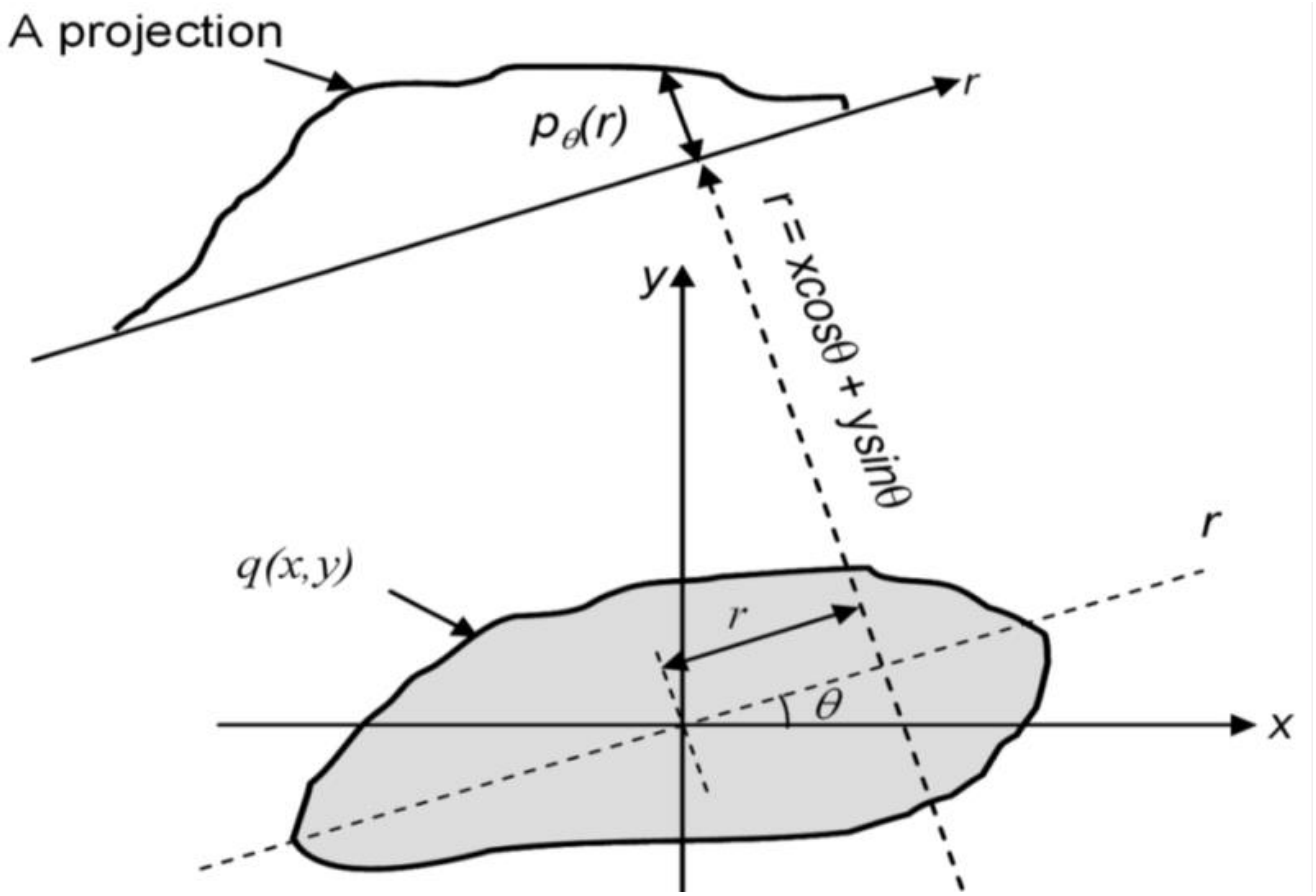

Figure 1: Projection of a 2D function, *q(x, y)*.

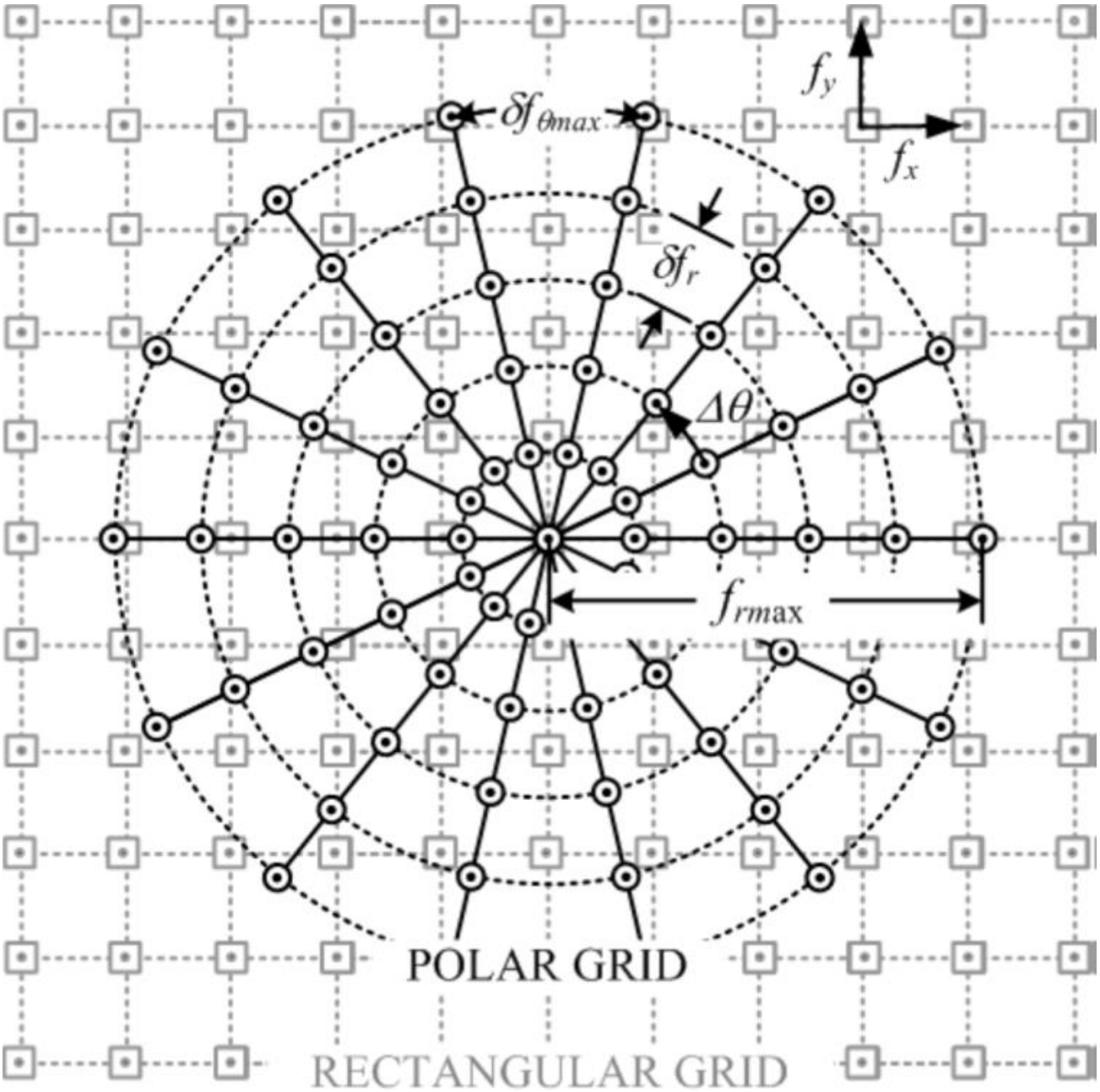

Figure 2: Polar grid (for data) and rectangular grid (for 2DIFT).

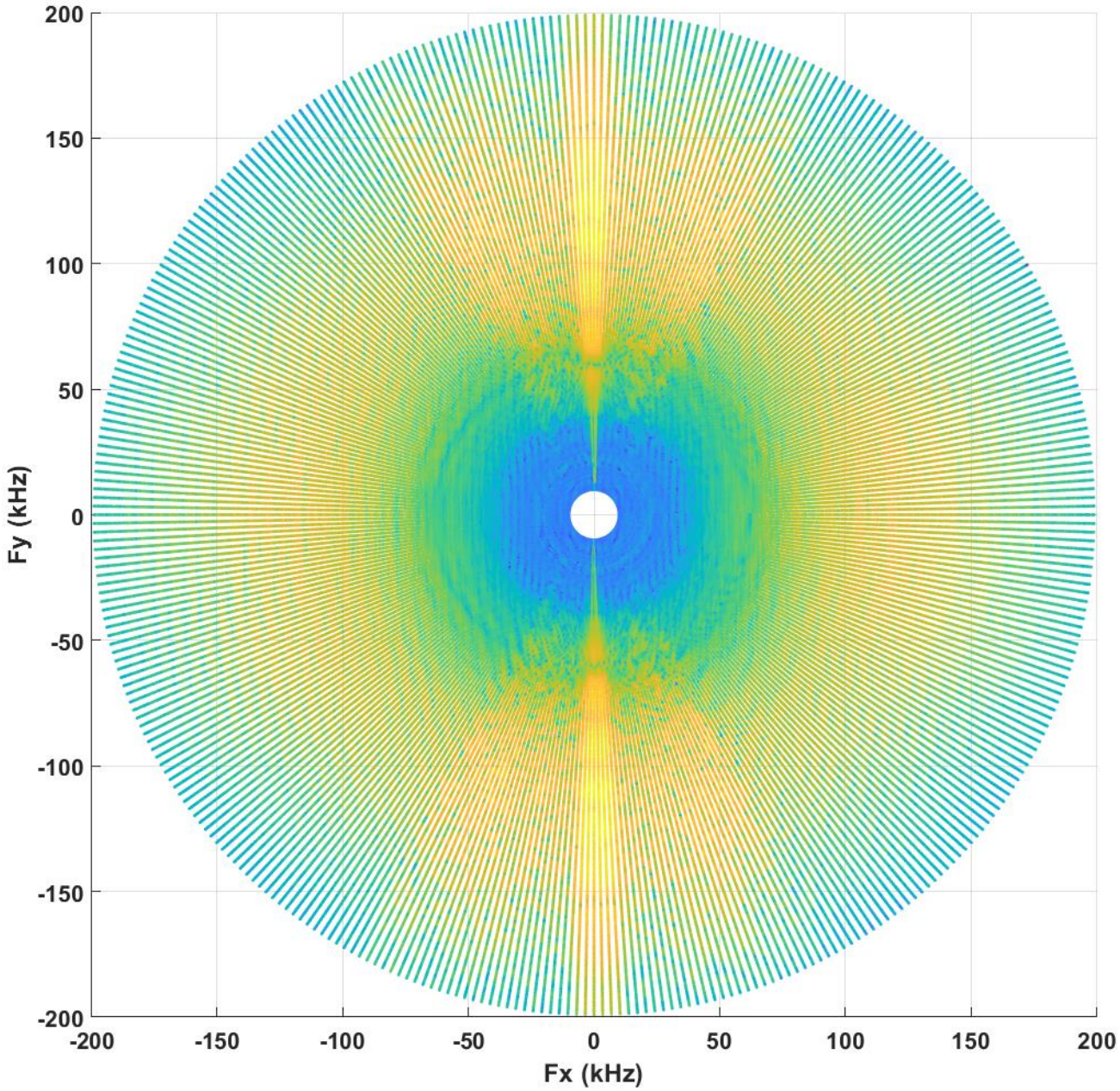

Figure 3: Spatial frequency domain.

3 EXPERIMENTAL DEMONSTRATION

3.1 Experimental Setup

Scattering experiments were conducted in a sonar laboratory consisting of a large water tank, acoustic transmitting and receiving modules and a motion system with several servo and stepper motors that move and rotate test objects. All modules are driven by a host controller as shown in Figure 4. The first test object was a solid granite cylinder with hemispherical end caps 550 mm long and 74 mm in diameter shown in Figure 6. The second object was a model of a generic submarine 692 mm long with a hull diameter of 86.2 mm. It is constructed from 0.3 mm brass shim using a few simple shapes including a hemispherical bow, cylindrical hull, cone-shaped tail and air-foiled shaped sail and control surfaces shown in Figure 6. The object under test was located at a distance of 4.0 m from the transmitter and automatically rotated about its vertical axis in 1° increments using the motion module which was fully automated and controlled by the host controller. The input signal was transmitted

repetitively with a ping interval of 100 ms and a duration of 86 µs to cover an upsweep frequency spectrum between 10 kHz and 200 kHz. A Butterworth filter was used to compress the input pulse minimising reverberation and reflection effects which can be particularly severe inside the relatively confined environment of the water tank. It was also important to use short input pulses for optimum object image resolution. The objects under test were rotated while ensonified by short sonar pulses. For each aspect angle of the objects, the scattered echo was recorded as a function of time (/distance). Distance from the transducer to the centre of rotation of the object was fixed. Any relative movement was compensated for prior to the next stage of tomographic translation. Any small error in this step could result in phase distortions and blurring of image formation. (Tran, Nguyen, at el, 2013)

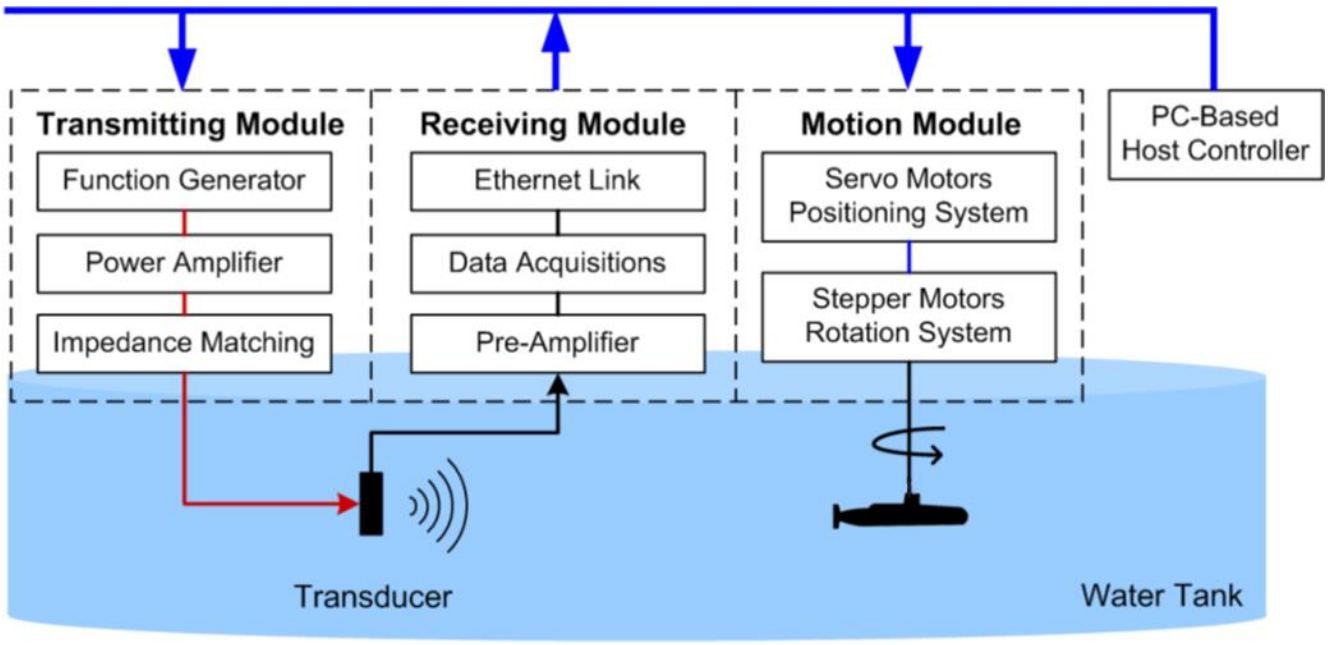

Figure 4: Schematic diagram of sonar laboratory.

Figure 5: Granite cylinder model.

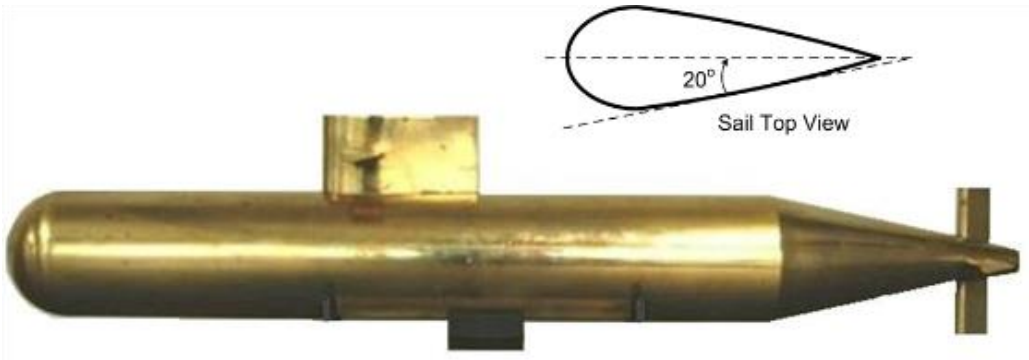

Figure 6: Brass generic submarine model.

3.2 Data Collection and Pre-processing

The scattered echo returns from the object were sampled at a rate of 6.25 MSamples/s. The collected data are single-channel real samples $s(k, t_n)$, where k, n respectively denote sonar echo index and time index in each pulse. To reduce transient and noise effects at each aspect angle, multiple scattered echoes were digitised and averaged over k. Prior to tomographic processing, a decimation of 4:1 was applied to raw data to reduce the sampling rate to 1.5625 MSamples/s; this is because the available signal bandwidth was not wide enough to necessitate the high sampling rate, and to reduce the computational cost. The final pre-processing step was matched filtering in the frequency domain to reduce spectral leakage. Matched filtering was used to optimise the achievable SNR by convolving raw data with the input signal measured at the location of the test object. Mathematically, the matched filter processing is expressed as

$$p_\theta(t) = \mathcal{F}^{-1}\{S_{tx}(f)\, S_{rx}(f)\}, \tag{6}$$

where $p_\theta(t)$ is a compressed range profile at aspect angle θ, $S_{tx}(f) = \mathcal{F}\{s_{tx}(t)\}$ and $S_{rx}(f) = \mathcal{F}\{s_{rx}(t)\}$ are the Fourier transforms of the transmit signal $s_{tx}(t)$ measured at the object's location and the received signal $s_{rx}(t)$ respectively.

4 RESULTS

For each received signal at a particular aspect angle, a projection was obtained indexed by the object's angular position. A collection of projections over a range of aspect angles is referred to as a spectrogram and these intermediate results for the granite cylinder and the brass generic submarine are shown in Figure 7 and 8 respectively.

The projections were then tomographically processed: the Fourier transforms of all available projections are placed in the spatial frequency space, at their corresponding aspect angles θ, followed by image inversion. The imaging results are shown in Figure 9 and 10.

5 DISCUSSION

One of the most striking features here are the helical elastic waves near the 'broadside' aspect angles of 90° and 270°. These are due to the excitation and re-radiation of helical compressional and shear waves along the cylindrical shell. The resonances occur when one round-trip phase increment along the shell circumference equals an integer multiple of 2π. These resonances contribute to the background noise of the tomographic images. Ideally, a pre-processing step to reduce these resonances should be performed prior to image inversion. The domination of the two specular reflections at broadside results in the formation of streaks across the tomographic images in the Polar-Coordinate BPA and the NUFFT BPA. The effect is less pronounced, and in fact, negligible in the Rectangular-Coordinate BPA, as clearly shown in Figure 9 and 10.

Overall, the Rectangular-Coordinate BPA performs more robustly in producing cleaner images in comparison to the Polar-Coordinate BPA counterpart but undoubtedly the NUFFT BPA produces a more pronounced and clear tomographic image.

Computational times on a standard PC running MATLAB for the three techniques are shown in Table 1. It is clear that the time required for calculation of NUFFT algorithm is far superior in comparison to other BPAs. Processing speed is especially important when dealing with a larger number of computations such as tomographic imaging.

Table 1: Computational time

Algorithm	Time (sec)
Polar	495.252
Rectangular	4.673
NUFFT	0.1964

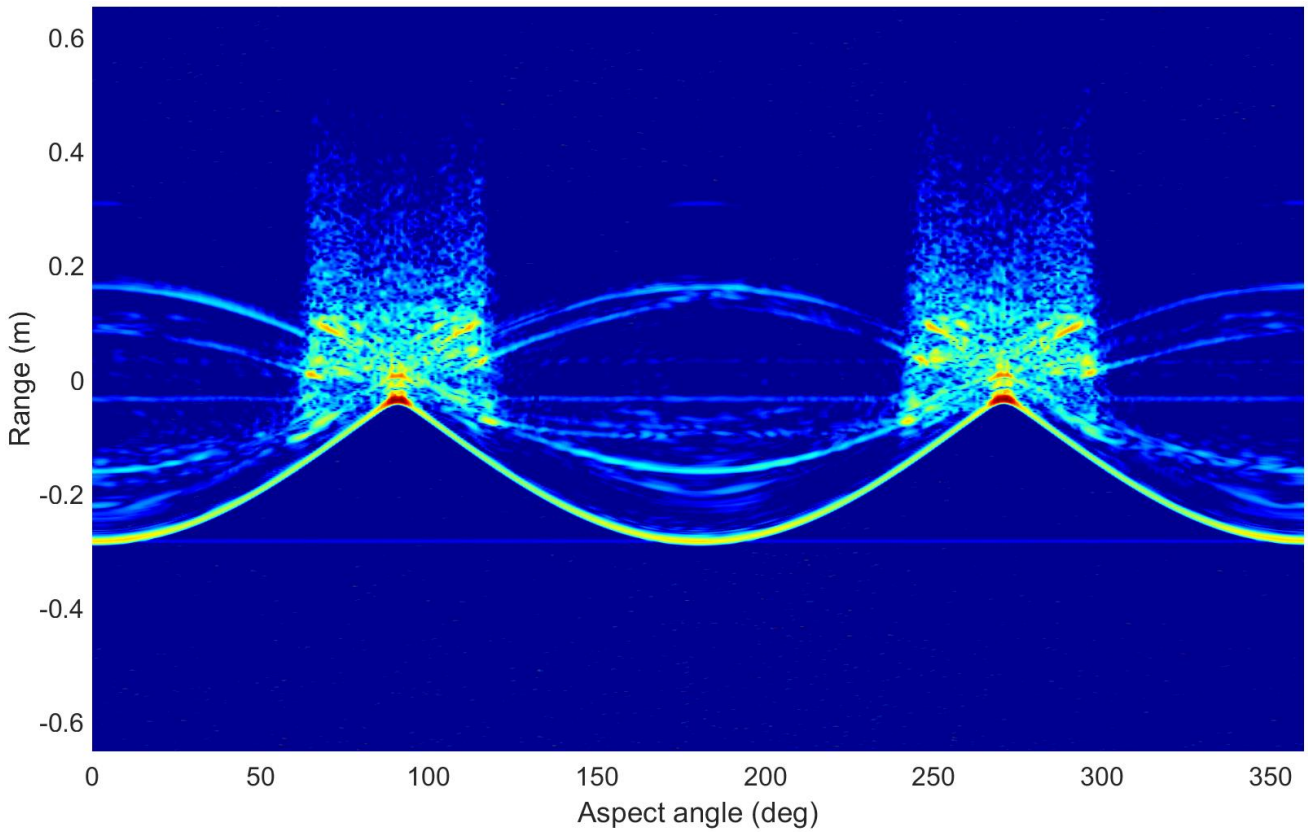

Figure 7: Spectrogram of the granite cylinder.

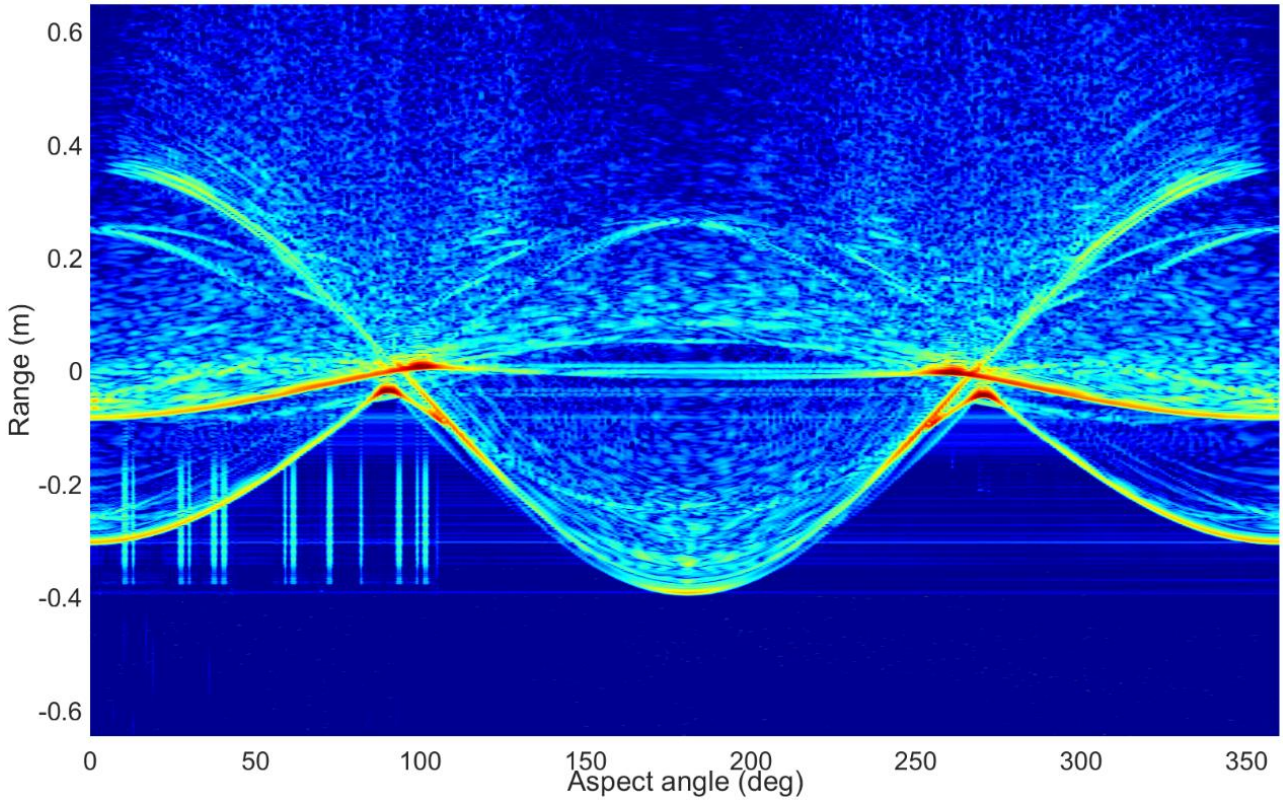

Figure 8: Spectrogram of the brass generic submarine.

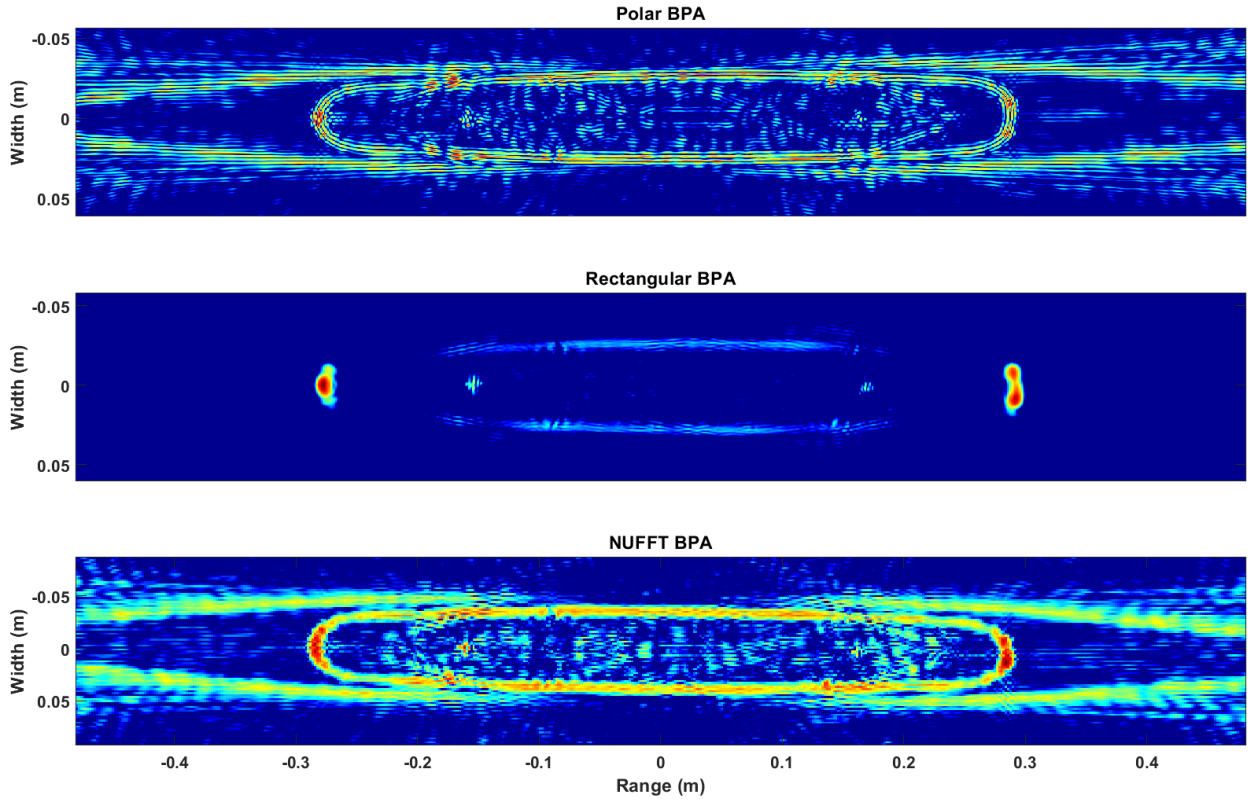

Figure 9: Tomographic images – granite cylinder.

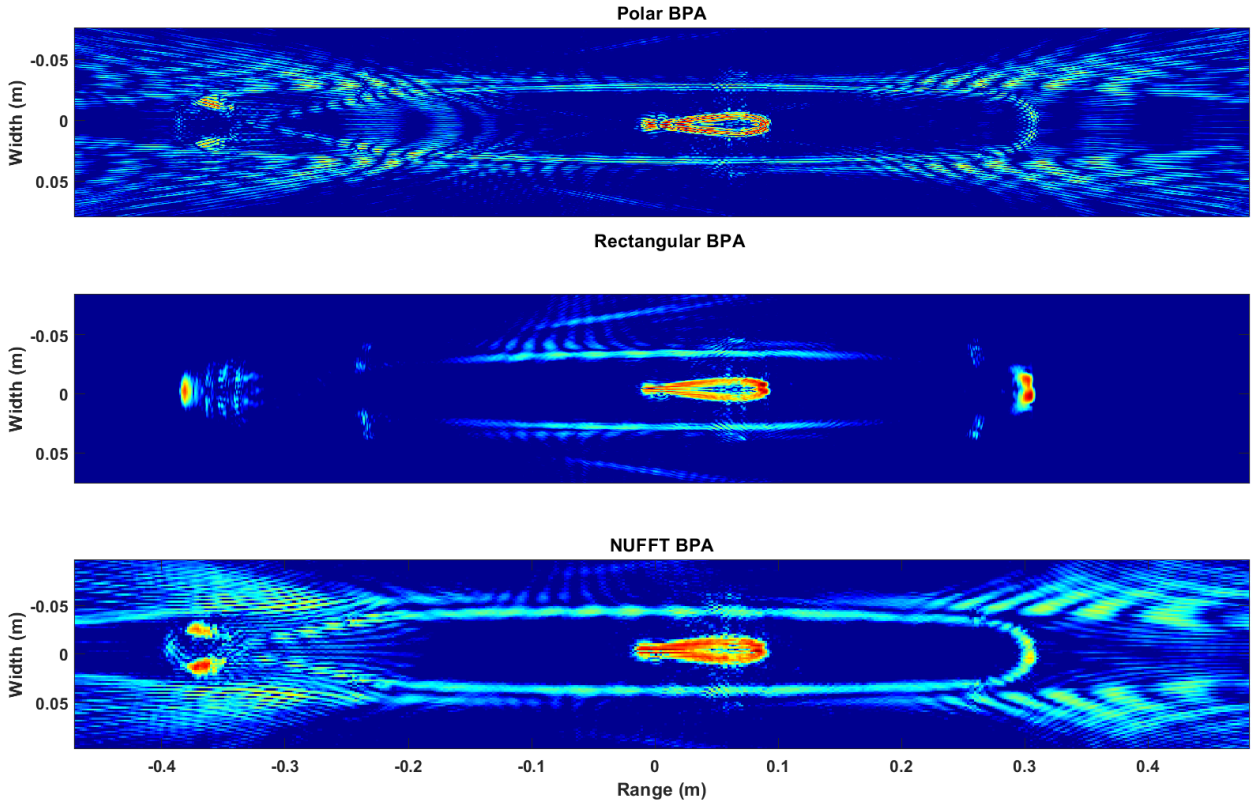

Figure 10: Tomographic images - brass generic submarine.

6 CONCLUSION

Sonar tomography is potentially a very powerful tool to visualise underwater objects. We have produced images of small objects ensonified at high frequency in a controlled laboratory environment. We have compared the performances of the NUFFT Back-Projection versus the Polar-Coordinate Back-Projection and the Rectangular-Coordinate Back-Projection algorithms used in the tomographic processing and found that the NUFFT BPA gives clear and defined images and is computationally efficient. Nevertheless the Polar-Coordinate and Rectangular-Coordinate BPAs can provide imagery that is complementary to the NUFFT BPA and combining these results may be considered for further improvement. Future work may include:

(i) an extension to multi-static sonar tomography using the NUFFT BPA algorithm and
(ii) a development of a real-time prototype system to image sonar echo returns.

REFERENCES

Tran HT., Nguyen B., Melino R., Wood S., 2013 "*A Detailed Study of Sonar Tomographic Imaging*", DSTO-RR-0394.

Monnig C. A., Marshall K. A., at el. 1988, "*Tomographic Image Reconstruction Technique For Spectroscopic Sources: Theory and Computer Simulations*", Office of Naval Research, Technical Report No. 36.

Kak A.C., M. Slaney, "Principles of Computerized Tomographic Imaging", Society of Industrial and Applied Mathematics, 2001.

Greengard L., Lee J. Y., 2004, "*Accelerating the Non-uniform Fast Fourier Transform*", Society for Industrial and Applied Mathematics, Vol. 46, No. 3, pp 443-454.

Matej S., Fessler J. A., Kazantsev I. G., 2003, "*Iterative Tomographic Image Reconstruction Using Fourier-Based Forward and Back-Projectors*", IEEE.